Author(s): Alaranta, Johanna M.; Truong, Khai-Nghi; Matus, María F.; Malola, Sami A.;
Rissanen, Kari T.; Shroff, Sailee S.; Marjomäki, Varpu S.; Häkkinen, Hannu J.;
Lahtinen, Tanja M.

Title: Optimizing the SYBR green related cyanine dye structure to aim for brighter nucleic acid
visualization
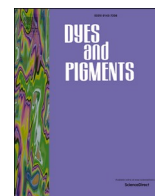
Please cite the original version:

Alaranta, J. M., Truong, K.-N., Matus, M. F., Malola, S. A., Rissanen, K. T., Shroff, S. S.,
Marjomäki, V. S., Häkkinen, H. J., & Lahtinen, T. M. (2022). Optimizing the SYBR green related
cyanine dye structure to aim for brighter nucleic acid visualization. Dyes and Pigments, 208,
Article 110844. https://doi.org/10.1016/j.dyepig.2022.110844

Optimizing the SYBR green related cyanine dye structure to aim for brighter nucleic acid visualization

Johanna M. Alaranta [a], Khai-Nghi Truong [a], María Francisca Matus [b], Sami A. Malola [b], Kari T. Rissanen [a], Sailee S. Shroff [c], Varpu S. Marjomäki [c], Hannu J. Häkkinen [a,b], Tanja M. Lahtinen [a,*]

[a] *University Of Jyväskylä, Department of Chemistry, Nanoscience Centre, Jyväskylä, P.O. Box 35, FI-40014, Finland*
[b] *University Of Jyväskylä, Department of Physics, Nanoscience Centre, Jyväskylä, P.O. Box 35, FI-40014, Finland*
[c] *University Of Jyväskylä, Department of Cell and Molecular Biology, Nanoscience Center, Jyväskylä, FI-40014, Finland*

A B S T R A C T

In recent years, the studies of RNA and its use for the development of RNA based vaccines have increased drastically. Although cyanine dyes are commonly used probes for studying nucleic acids, in a wide range of applications, there is still a growing need for better and brighter dyes. To meet this demand, we have systematically studied the structure of SYBR green-related cyanine dyes to gain a deeper understanding of their interactions with biomolecules especially how they interact with nucleic acids and the structural components which makes them strongly fluorescent. Herein, five new dyes were synthesized, and their photophysical properties were evaluated. Observations of photophysical characteristics were compared to calculations by using density functional theory in its ground state and time-dependent form to model the optical absorption spectra and excited state properties of the selected molecules. Single crystal X-ray crystal structures of five cyanine dyes were determined and the interactions of the cyanine dye-DNA complex were studied by using molecular docking and molecular dynamics calculations. Three molecular structural features were discovered: a) removing the benzene ring from the thiazolium moiety of the dye lowers the fluorescence drastically, and that the quantum yield can be enhanced, therefore increasing the fluorescence, by b) incorporating methanethiol substituent at the quinoline moiety instead of dimethylamine or c) changing the thiazolium moiety to an oxazolium moiety.

1. Introduction

Cyanine dye studies are nowadays widely focused on biological and medicinal research. New potential uses for cyanine dyes are for example cancer treatment [1–3], nanofibers mimicking tissues [4], detecting cysteine, which is linked to many illnesses, such as Alzheimer's disease [5], turn-on probes for redox reactions in cells [6] and using cyanine dyes as selective fluorescent probes for RNA [7]. Cyanine dyes are already a popular choice as fluorescent probes to image nucleic acids in many cell and molecular biology laboratories [8]. In the field of cyanine dyes the monomethine cyanine dyes are one of the most used fluorescent probes for visualizing nucleic acids in different applications due to their fluorescence enhancement when binding to nucleic acids [9].

Cyanine dyes can be defined as molecules containing two nitrogen substituted heterocycles sharing a cationic charge through a conjugated carbon bridge [10]. Monomethine cyanine dyes are one class of the cyanine dyes, given the name due to only one monomethine carbon in the carbon bridge [11]. A classical way to synthesize monomethine cyanine dyes is the cyanine condensation reaction of two quaternary amine salts [12]. Molar absorptivity of these compounds usually range from 10^4–10^5 cm^{-1}M^{-1} and they can exhibit up to 1000-fold increase in fluorescence intensity when binding nucleic acids. Due to these excellent qualities, this host-quest type of interaction between the cyanine dyes and nucleic acids is widely utilized in different applications [10].

The great fluorescence enhancement of cyanine dyes is described as a result of restriction of the torsional motion of the molecule. The group of Geddes [13] has shown that both PicoGreen and SYBR Green I form a complex with double stranded DNA (dsDNA), in which the aromatic quinolinium core unit intercalates into the dsDNA, while the benzo-thiazolium unit, carrying a localized positive charge enhances the

---

binding affinity by providing additional electrostatic interaction with the DNA. In addition, the dimethylaminopropyl side chains are positioned in the minor groove of the DNA for added stability of the complex. Another possible binding mode is minor groove binding where the whole dye molecule binds in minor grove of the dsDNA. For example, Karlsson et al. [14] reported two minor groove binding unsymmetrical cyanine dyes also suitable for DNA detection.

Knowledge of the binding and structural modifications to the brightness of these dyes is mostly based on a few examples. However, for the future development of more selective and efficient dyes that enable the study of more complex biological systems (*e.g.* viruses and their mode of action in living cells), it is highly significant to understand the structural and binding properties of the cyanine dye molecules. Since these fluorescent probes must have some particular features to be useable for sensing applications: high brightness combined with low background emission, high photostability under prolonged excitation, and low cytotoxicity when applied *in vivo*, it is important to understand how the structures of these dyes can be modified without losing these features but still exhibit a new quality.

The aim of this study is to reveal the key factors that improve the behavior of the monomethine cyanine dyes as fluorescent probes for nucleic acid staining. To accomplish this, we made systematic modifications to quinoline, benzothiazolium, and -oxazolium moieties around the fixed core fluorophore skeleton of different SYBR green-related monomethine cyanine dye molecules. Five new monomethine cyanine dyes (**1–5**) were prepared and their photophysical properties compared with other known dyes (**6–9**) of the same family using fluorescence and UV–Vis spectroscopy. For selected dyes (**1**, **2**, **6**, **8**, **10a** and **10b**, X-ray crystal structures were determined, and their potential DNA binding modes were studied by molecular modeling.

2. Materials and methods

All used reagents and materials were commercially available and used as received unless otherwise mentioned. All dyes were synthesized with a modified and developed synthesis method previously published by our group [15] based on protocols found in literature [16,17].

2.1. Synthesis

All of the studied dyes (**1-10**) were synthesized by first introducing

quinolone or pyridine **11** to phosphorus oxychloride to get positively charged ions **12** (see Scheme 1). After that cyanine condensation reaction was done as described by Karlsson et al. [18]. This resulted in a mixture of dyes with chlorine and methyl thiol substituents in pyridine or quinoline moiety. After separation, thiol dyes can be used as such, and chlorine dye can be mixed with dimethylamine to obtain amine dyes.

The synthesis procedure is very versatile, and it can be used with differently substituted starting materials as seen in Scheme 1. All new cyanine dyes are presented in Fig. 2. along with the dyes previously published [15].

2.2. Analytical methods

Synthesized dyes were characterized using mass spectrometry and NMR spectroscopy. NMR spectra were measured with Bruker Avance III 500 MHz NMR spectrometer. Agilent LC-IMMS-TOF mass spectrometer was used to determine accurate mass for each dye.
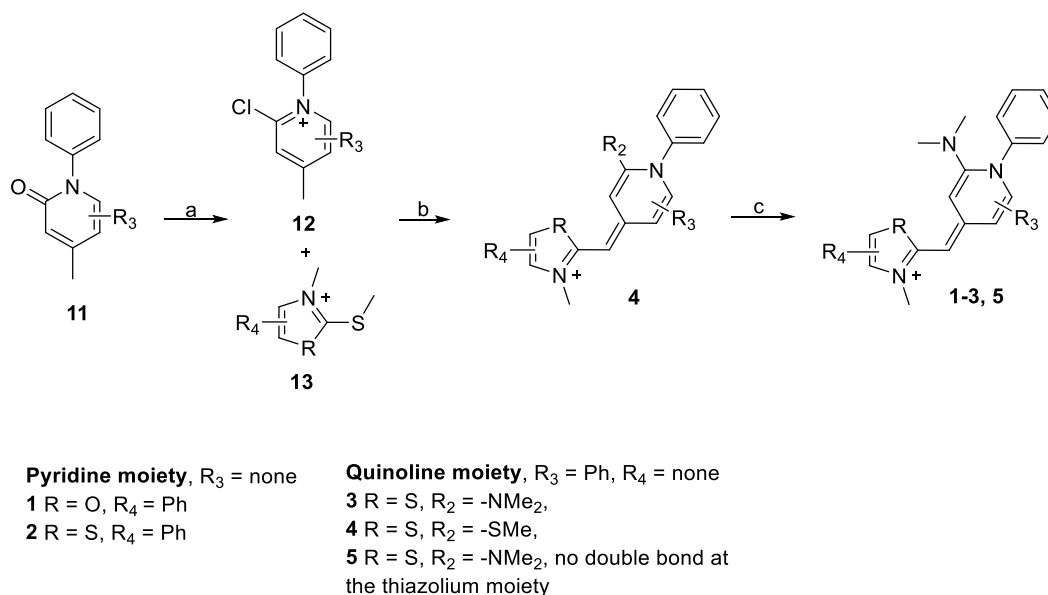
Photophysical properties of the dyes were measured with UV–Vis and fluorescence spectrometers. Agilent Technologies Cary 8454 was used to measure absorbance and Varian Cary Eclipse for fluorescence studies.

Atomic coordinates and structure factors for the reported crystal structures have been deposited with the Cambridge Crystallographic Data Centre (CCDC) under accession numbers 2194823 (PyrON **1**), 2194824 (PyrN **2**), 2194825 (OxN **6**), 2194826 (ThzN **8**) and 2194827 (**10**, see Scheme S10.).

For comprehensive synthetic and experimental details please see the Supporting Information.

3. Results and discussion

In this study, we have synthesized five new nucleic acid-binding cyanine dyes to study how different functional groups affect to the nature of the quality of the dyes in photophysical measurements. In our previous paper, we concluded that a single heteroatom could change the qualities of the dyes drastically and oxazolium moiety seemed to produce better dyes [15]. With that in mind, we were interested to see the effect of the thiazolium moiety. Therefore, we present the new S-series of dyes containing thiazolium moieties with modified structures. We set our goal to study the structures of these cyanine dyes to see if the aromatic rings in the molecules have an essential role in the brightness and

Pyridine moiety, R₃ = none
1 R = O, R₄ = Ph
2 R = S, R₄ = Ph

Quinoline moiety, R₃ = Ph, R₄ = none
3 R = S, R₂ = -NMe₂,
4 R = S, R₂ = -SMe,
5 R = S, R₂ = -NMe₂, no double bond at the thiazolium moiety

Scheme 1. Synthesis scheme for studied dyes. Reagents: a) POCl₃, 1.2-DCE, Δ b) DCM, Et₃N c) Chlorine dye from previous step, HNMe₂, ACN.

DNA binding modes. Trusting the results will open new ideas for developing dyes in the future. The five new synthesized cyanine dyes and selection of the commercial cyanine dyes were compared to our previously published cyanine dyes [15] to get deeper information on how these modifications affect the fluorescence behavior.

The R_3 represents the benzene ring for dyes with quinolone moiety, while for pyridine moiety, there is no R_3 substituent. Thiazolium and oxazolium dyes have sulfur and oxygen as R atom, respectively (see Scheme 1). Accordingly, these two different groups of dyes are represented as sulfur and oxygen series in Fig. 2. The arm R_2 can be either methyl thiol or dimethylamine.

The currently accepted model for interaction between SYBR green-related dyes and dsDNA is based on the intercalation of quinoline moiety (red circle in Fig. 1.) between the base pairs in the double helix. Thiazolium/oxazolium moiety (blue circle in Fig. 1.) bears the positive charge, and hence, provides electrostatic interactions with the negatively charged phosphate groups in the nucleic acid backbone. The arms (green circle in Fig. 1.) could bind along the helix with minor or major groove, and therefore it enhances the binding [13].

3.1. X-ray crystallography

The crystallization of dyes **1–9** and separation of **10a** and **10b** (see Scheme S10) were attempted, but crystals with suitable quality for single crystal X-ray structural analysis resulted in only for dyes **1**, **2** (a mixed crystal, see Fig. 3), **6**, **8** and **10** (a mixed crystal, see Scheme S10. and Fig. S15) and X-ray structures are shown in Fig. 3. The crystal data and other experimental details are given in SI. The main molecular skeleton (oxazolium/thiazolium moiety and quinoline/pyridine moiety) of all dyes is nearly planar in the solid state, despite the fact that it appears to be non-planar in solution. Only the dimethylamine (-NMe$_2$) arm and the phenyl group attached to the main skeleton deviate from the planarity due to their close proximity. The configuration of **2** in the solid state differs from all other dyes. Using O/N atom of the oxa/thia moiety and the -NMe$_2$ or -SMe arms as substituents of the C=C moiety (Fig. 3.), then **2** is defined as *cis*, while all other dyes have a *trans* configuration. In dye **6** (the best performing dye from the studied dyes), the -NMe$_2$ arm (which is planar too) has a twist/torsion angle of 20.7° while the phenyl group is nearly perpendicular towards the plane of the main skeleton of the molecule (twist angle of 77.4°). The other dyes containing the -NMe$_2$ arm have similar twist angles: **1**, 33.1° and 53.9°; **2**, 42.8° and 65.0° and **8**–35.6°, −64.6°. The commercial dye, **SYBR Green II** and **MeS**, which have R–S arm instead of -NMe$_2$, differ from the above as the R–S group is co-planar with the main skeleton and the phenyl ring twist angle is closer to 90° (**MeS** 79.3° and **SYBR Green II** 88.1°). The overall structure of these dyes is very similar (see the VDW radii plots in the SI, Fig. S16). The major structural difference affecting the brightness of the dye is the thiazolium moiety. The longer C–S bonds, 1.74 Å *vs.* 1.37/1.39 Å opens the C=C–C angle between the oxa/thia moiety and quin/

py moiety angle from 125° to 128°. In addition, the larger 5-membered thiazolium ring induces a change in the mutual orientation of the oxa/thia and quin/py moiety of the dye. The cent1 – Csp2 – cent2 angle (cent1, Csp2 and cent2 being the centroid of the oxa/thia benzene ring, the alkene carbon, and the centroid to the benzene ring of the quin/py moiety, respectively) in the thiazolium moiety-containing dyes opens up by 10°, being 137.8° in **2** and 136.2° in **8**. In the oxazolium moiety-containing dyes, the same angle is 127.4°, 126.4°, 124.1°, and 126.8° for **1**, **6**, **SYBR Green II**, and **MeS**, respectively.

3.2. Photophysical studies

Photophysical properties of dyes (**1–9**) were evaluated with UV–Vis- and fluorescence spectrometers. For the molar absorption coefficient, series of absorption titrations were done for each dye in EtOH, TE buffer and ctDNA in TE buffer solution to visualize the linear correlation between the concentration and the absorbance [19]. For the fluorescence measurements, titrations were measured in excess ctDNA in TE buffer (100 μM solution) and in restricted ctDNA concentration (0.52 μM). These fluorescence titrations were used to estimate the binding properties of the dyes according to the McGhee Von Hippel equation [20]. The quantum yields of the dyes were determined by comparing the dyes to fluorescein standard by exciting the studied dyes and the fluorescein at same wavelengths regardless of the previously measured maxima. Resulting emission spectra were integrated and plotted against absorbance maxima at the used excitation wavelength. Slopes of these linear plots were then used to determine the quantum yields for the dyes [21].

All dyes (**1–9**) absorb light at different wavelengths which can be seen from Fig. 4., ranging from 466 to 511 nm. Some correlations on the absorption maxima depending on the structures of the dyes can be seen from the plot. The dyes with benzothiazolium moiety (ThzS **9**, ThzN **8** and PyrN **2**) seem to absorb at higher wavelengths than dyes containing oxazolium moieties; dyes **9**, **8** and **2** have maxima at higher wavelengths compared to MeS **7**, OxN **6** and PyrON **1**. Similar observations have been made by Benson and Kues [22]. The dyes with thiol arm, **7**, **9** and QuinoS **4** absorb at higher wavelengths than the amine arm containing dyes, **6**, **8** and QuinoN **3**. Also removing benzene ring from quinoline moiety, lowers the absorption wavelength for dyes **1** and **2** compared to dyes **6** and **8** with the benzene ring attached to quinoline, respectively. Same trend goes to the quino dyes (**3–5**) where the benzene ring has been removed from the thiazolium moiety. QuinoN **3** and QuinoN-2 **5** absorb at lower wavelengths than dye **8** and similarly dye **4** at lower wavelength than dye **9**. Quite interestingly, dyes seem to have different peak shape depending on which arm they have. Thiol containing dyes (**4**, **7** and **9**) show a shoulder, a bit smoothed out in dye **7** but still visible which cannot be seen for amine dyes (**1–3**, **5**, **6**, **8**). Same trends were expected to be observed in emission spectra of all studied dyes.

Peaks are more overlapping in normalized emission spectra compared to absorption spectra above. Emission maxima range from
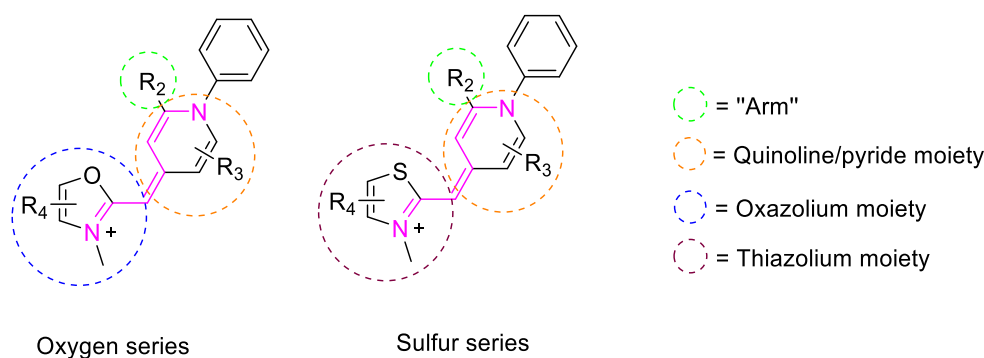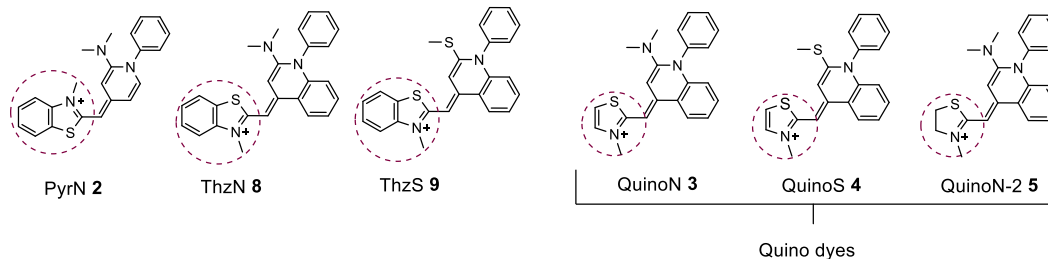

Fig. 1. Schematic picture of studied dyes with explanations for different structural moieties. The common fixed core skeleton found in all cyanine dyes is highlighted with magenta.

Sulfur series (S-series)

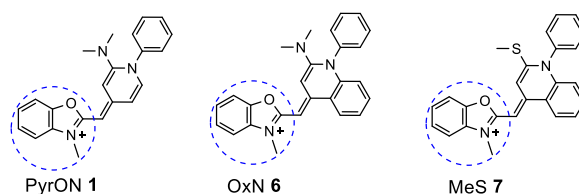**Fig. 2.** Structures of newly synthesized (**1–5**) and previously published (**6–9**) [15], [17] dyes.
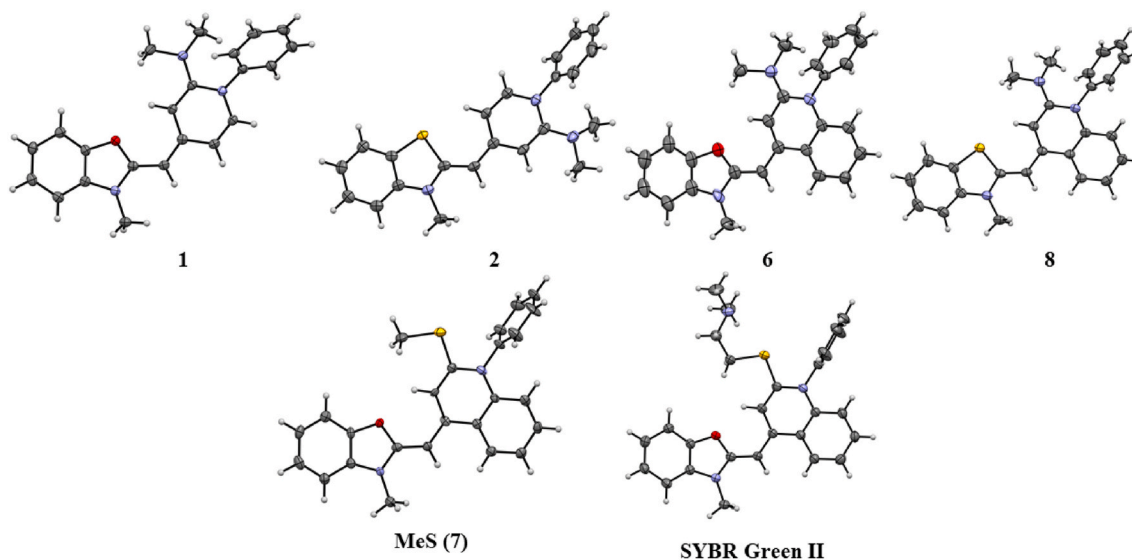

Fig. 3. The X-ray structures of dyes **1, 2, 6, 8** (top) and the commercial dyes **MeS** and **SYBR Green II** (below). Anions and solvent molecules are omitted for clarity.

436 nm to 514 nm, a bit wider range compared to absorption maxima. In Fig. 4., same trends observed in absorbance plot can be seen; dyes with benzothiazolium moiety (**2, 8, 9**) emit at higher wavelengths compared to dyes with oxazolium moiety (**1, 6, 7**). As also observed in absorption spectra, dyes with thiol arm (**4, 7, 9**) emit at higher wavelengths compared to the amine dyes with otherwise same structure (**3, 6, 8,**). Removing benzene from either thiazolium or quinoline moiety lowers the emission wavelengths for studied dyes. Dyes **1** and **2** emit at lower wavelengths compared to dyes **6** and **8**. Similarly, Dye **4** emits a bit lower compared to compound **9**. Biggest difference between emission maxima when benzene have been removed can be seen for compound **5** compared to dye **8**. Dye **5** emits 44 nm lower than **8**, when second biggest difference between dyes **6** and **1** is 27 nm. Surprisingly, dye **3** emits 1 nm higher than compound **8** being the only exception to the trend observed. Line shapes for compounds **3** and **4** are not as smooth as

other dyes due to low intensities even at high dye concentrations. To be able to understand how the dyes behave in more detailed manner series of titrations were performed to obtain molar absorption coefficients in various solvents.

Molar absorption coefficients, ε_{max}, were measured for each dye in three different solvents: TE buffer, ctDNA and ethanol. Ethanol was chosen as organic solvent to see if water solubility has effect in the absorption. Molar absorption coefficient is based on Beer-Lambert law:

$$A = \epsilon l c$$

Where ϵ = molar absorption coefficient, l = path length in cm (usually 1 cm) and c = concentration of the studied molecule. Hence, the molar absorption coefficient describes the correlation between the measured absorption and the concentration of the sample [19].

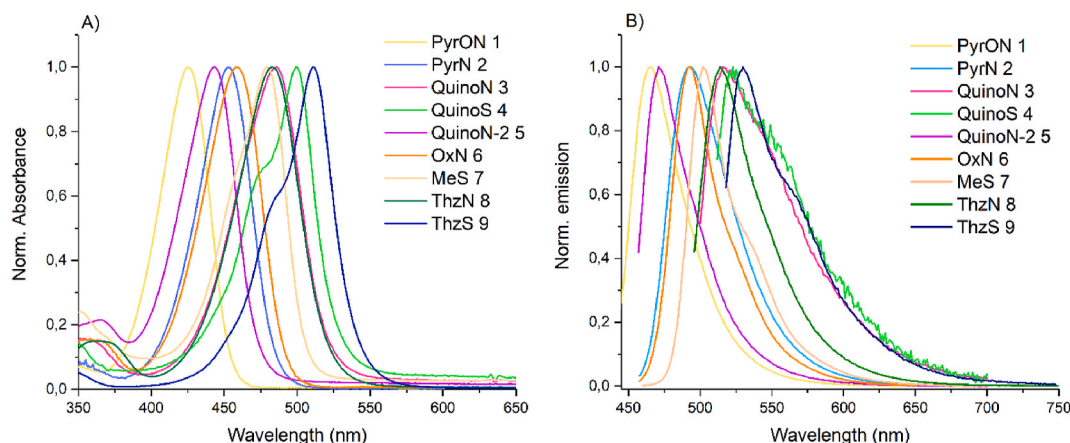Absorption coefficients between studied dyes vary depending on the

Fig. 4. A) Normalized absorptions of all dyes (**1–9**) in EtOH. B) Normalized emissions of all dyes (**1–9**) in 100 μM ctDNA solution. Dyes were excited with the excitation maxima unique to each dye: **1** at 436 nm, dye **2** at 463 nm, dye **3** at 492 nm, dye **4** at 505 nm, dye **5** at 449 nm, dye **6** at 464 nm, dye **7** at 487 nm, dye **8** at 488 nm and dye **9** at 514 nm.

structures and used solvents. From Table 1. no clear correlation can be seen between the dye's structures and the magnitude of absorption coefficients. All dyes, however, exhibit the highest absorption coefficients in ethanol. This indicates that when dyes are fully soluble in a certain solvent, the absorption enhances. Dyes **3** and **4** show the lowest absorption coefficients throughout the measurements regardless of the solvent. Compound **5** has two-folds higher values compared to dye **3** due to the missing double bond. Dyes **1** and **2** have similar absorption coefficient values compared to dyes **6** and **8**, the latter containing the benzene ring in pyridine moiety. When imagining biological samples, a clear difference between the excitation and emission maxima is preferred to avoid self-quenching of the emission peak. Hence Stoke's shifts were calculated and compared.

Stoke's shifts seemed to have a correlation to the structure of studied dyes. In the dyes **6–9** this correlation was already observed; dyes with thiol arm, **7** and **9** and also the new dye **4,** have smaller Stoke's shifts compared to the dyes with amine arm (**1–3, 5, 6, 8**). However, the Stoke's shifts of dyes **3** and **5** with amine arm are not significantly higher compared to dyes with thiol arms (**4, 7** and **9**) but the overall trend can still be seen. Similar enhancement of Stoke's shift was also found by Zhang et al. [23] and Peng et al. [24] when replacing chloride by amine group. The same was also observed in our previous studies [15]. Together with the Stoke's shifts, quantum yield is an important way to evaluate fluorescent probes since it tells how much of the absorbed photons are emitted and therefore it can illuminate which dyes could be potentially strongly fluorescent.

Quantum yields of the dyes were evaluated by comparing them to the fluorescein standard. Dye **6** was determined to have a quantum yield of 100% and the new dye **1** is a match to it, also exhibiting a quantum yield of 100%. These compounds have similar structures, except for the absence of the benzene ring in the quinoline moiety in dye **1**. Therefore,

similar result was expected for compound **2** when compared with dye **8**. Interestingly, quantum yield for dye **2** is 10% lower than compound **8** even though the only difference between these two structures is the benzene ring missing from the quinoline moiety. With these results, we expected to observe quantum yields in same region for Quino dyes (**3–5**) compared to similar dyes with benzene rings at thiazolium moiety. Surprisingly, removing the benzene from thiazolium moiety lowered the quantum yields severely, biggest difference being 65.3% between dyes **8** and **3**. This result indicates that the benzene ring at thiazolium moiety has important role to the dyes and their photophysical properties.

All studied dyes exhibit low background emission (see Fig. S21 and Fig. S22) in TE buffer without ctDNA presence. The best fluorescent enhancement was exhibited by dye **6**, of 1050 times, the similar value to commercially available dyes PicoGreen [13] and SYBR Green I [25]. Generally, fluorescent enhancements of the studied dyes were over 400 times for the dyes with the best quantum yields (over 50%) and similarly, dyes with poor quantum yield (lower than 15%), also exhibited lower fluorescent enhancement, maximum of under 300 times. Thus, the relation with the fluorescent increasement and quantum yield is noticeable. However, high quantum yield does not automatically mean high fluorescence enhancement, the dye **1** with quantum yield of 100% exhibited fluorescent enhancement only of 414 times due to the highest measured background emission. In order to get a more comprehensive understanding how useable probes the studied dyes are, also the brightness was determined for each dye.

Brightness was calculated for each dye to have a number describing their quality (complementing the molar absorption coefficient). Brightness is calculated by multiplying the molar absorption coefficient in the 100 μm ctDNA solution with the determined quantum yield. Dye **6** has the highest brightness, compound **1** being just a bit short with a brightness of 36100. Similarly, dye **2** is just a bit less bright than dye **8**.

Table 1
Spectral data measured from studied dyes, see Fig. S17.-Fig. S23. for related plots. Data for dyes **6–9** was taken from our previous article [15] to be compared with the dyes (**1–5**) here presented. Reported excitation maxima were used to record emission spectra and vice versa for each dye.

Dye	λ_{exc} (nm)	ε_{max} (TE Buffer)*	ε_{max} (EtOH)*	ε_{max} (100 μM ctDNA)*	λ_{emi} (nm)	Stoke's Shift (nm)	Φ (%)	Brightness ($M^{-1}cm^{-1}$)
PyrON **1**	436	59.4 ± 0.30	68.4 ± 0.50	36.1 ± 0.80	465	29	100	36100
PyrN **2**	463	40.3 ± 0.20	56.1 ± 0.14	30.8 ± 0.40	492	29	52.3	16000
QuinoN **3**	492	11.9 ± 0.12	19.7 ± 0.20	12.2 ± 0.02	516	24	2.8	431
QuinoS **4**	505	8.87 ± 0.14	14.4 ± 0.06	8.4 ± 0.10	523	18	2.2	264
QuinoN-2 **5**	449	22.5 ± 0.06	38.1 ± 0.30	20.1 ± 0.01	471	22	6.5	1310
OxN **6**	464	56.5 ± 0.80	73.6 ± 0.60	47.3 ± 0.20	492	28	100	47300
MeS **7**	487	16.0 ± 0.30	25.7 ± 0.30	18.0 ± 0.30	503	16	76.4	13800
ThzN **8**	488	47.53 ± 2.00	56.9 ± 0.40	36.5 ± 0.30	515	27	68.1	24900
ThzS **9**	514	35.3 ± 1.00	65.4 ± 1.10	49.1 ± 0.07	533	19	13.6	6700

*Unit for molar absorption coefficient in this table is x10^3 M^{-1}cm^{-1}

Quino dyes (**2–5**), however, show very low brightness compared to all other dyes. This result further indicated even that benzene ring at the thiazolium moiety has a key role in the structures since its remotion drastically lowers the brightness. However, the benzene ring can be removed from quinoline moiety without a major impact in the brightness. This could be due to the inductive effect of the benzene ring and positively charged nitrogen. Nitrogen with positive charge is an electron withdrawing group and hence it could withdraw electrons from the benzene ring to itself [26] When benzene donates electron density to the nitrogen, it could stabilize the positive charge of the nitrogen. However, the assignment of the local positive charge is uncertain since, based on the X-ray crystal structure studies, there is an indication of delocalization of this charge along the carbon chain between the two nitrogen atoms.

Next, the experimental observations of photophysical properties were compared to calculations. We used density functional theory (DFT) as implemented in code-package called GPAW and time-dependent density functional theory in linear response formalism (lr-TDDFT) to model the optical absorption spectra and excited state properties of the selected molecules [27] In all calculations we used real-space grids and Perdew-Burke-Ernzerhof (PBE) functional [28] Our calculations concentrated on two dyes from oxygen series: dyes **6** and **7** and one dye from sulfur series: dye **2**. Selected molecules comprise of higher and lower fluorescence efficiencies as well as have structural variation in the arm R_2 and in the R_3 and R_4 moieties. Calculated optical absorption spectra are shown in Fig. S26. In general, the calculated main peak positions (dye **6**, 417 nm; dye **7**, 431 nm; dye **2**, 399 nm), are systematically blueshifted by 0.3–0.4 eV as compared to experimental. Dye **2** absorbs with highest intensity at the shortest wavelengths from the three dyes whereas dye **7** absorbs at the longest wavelengths with the second highest intensity. Calculated absolute intensity of the weakest absorption peak of dye **6** is 83% of the strongest absorption of dye **2**. Despite of the systematic blueshift, the relative order of the peak positions is exactly the same as observed experimentally.

Emission properties were calculated by relaxing the excited states using finite differences method to the excited state energy within the lr-TDDFT framework. Excited states for the relaxation were selected based on the main absorption peak. Root mean square deviation (RMSD) per atom between optimized excited state and ground state structures is seen to be in a range of 0.083 Å - 0.108 Å, which means that all structures are rather static as visualized in Fig. S27. By visual inspection it can be noticed that there is slightly more out-of-plane deviation in the positions of the atoms in the excited state structures compared to ground state, but the differences are very small. Oscillator strengths of the lowest energy transitions of the relaxed excited states were then plotted as Gaussian broadened curves to mimic the emission spectrum which is visualized in Fig. S28. In contrary to the blueshift of the absorption peaks, the positions of the calculated emission peaks (dye **6**, 494 nm; dye **7**, 482 nm; dye **2**, 504 nm) are very close to the experimental (dye **6**, 492 nm; dye **7**, 503 nm; dye **2**, 493 nm). Remarkably, the absolute intensity of the emission peak of the dye **2** is 4–5 times lower than for dye **6** and **7**. This difference is in qualitative agreement with the experimental observed differences in fluorescence behavior, for example, the brightness. Calculated spectrum of dye **7** shows also a shoulder next to the main emission peak as observed in the experiments. Due to the systematic blueshift in the absorption peaks, also the calculated Stoke's shifts get radically overestimated, but their order is again the same as in the experiments, *i.e.*, compound **7** gives the largest and **2** clearly the lowest Stoke's shift from the three selected dyes. These calculated results give qualitative support to experiments and confirm observed trends in photophysical properties with respect to the structural modifications. Since the experimental and calculated emission and absorbance spectra were similar with only systematic shifts, the relationship between the dyes and ctDNA was studied even further by determining the binding parameters.

McGheen Von Hippel equation [20] was used to estimate binding constant (K_a) and binding site size (n) for each dye. Binding modes between the dyes and DNA were studied by measuring emission in two different ctDNA solutions, in excess ctDNA and 0.52 μM ctDNA solution. Then this data was plotted using the McGhee Von Hippel equation. From the binding constant K_a, dissociation constant (K_d) can be calculated which can be further used to calculate Gibbs free energies ($\Delta G°$) for the dyes. Results for K_a, K_d and $\Delta G°$ are presented in Table 2. Theory and application of this equation have been presented in a more detailed manner in an article published by our group [17].

Surprisingly results from McGhee Von Hippel plots show noticeable variation between studied dyes. Interestingly, dyes **3** and **4** which showed poor emission throughout the measurements, seem to bind tightly with DNA since the binding constants, K_a, for both compounds are in the same region as dye **6**, exhibiting strong emission with DNA. Also worth noting is the decrease in binding constant from 7.7 x 10^6 M^{-1} to 2.2 x 10^6 M^{-1} when the double bond from compound **3** is removed to get compound **5**. Dyes **3** and **4** have much smaller bindings site sizes compared to other new dyes, **1**, **2** and **5**. The binding site is two sizes larger for compounds **2** and **5** and four sizes larger for dye **1** when compared to the dyes **3** and **4**. This result would suggest that these dyes bind differently to the DNA. Dyes **6–9** show clear correlation between the binding constant and the brightness; dyes with higher binding constant, also showed better brightness, which is not observed for the dyes **1–5**. Interestingly dyes with low brightness (**3–5**) exhibit strong binding with DNA but they are not as emissive as dyes with looser binding. Compounds **1** and **2** have low binding constants, but they are still very emissive and are brighter than, for example, dye **7**. The latter exhibits two times higher binding constant compared to compound **2** and almost four times higher than dye **1**. Dyes **1**, **2** and **5** have lower binding constants, and they take effectively more space in binding sites compared to other dyes indicating that they do not bind as tightly to the DNA as for example dye **6**. As discussed in introduction, interaction mode between SYBR green related dyes and nucleic acids is described by the intercalation of quinoline moiety between the base pairs and the thiazolium moiety interacting with phosphate groups of the nucleic acids [13] or by the whole dye binding with the minor groove of the DNA [14]. Removing the benzene ring from the quinoline moiety makes the intercalator part and the whole molecule smaller; hence it might get too small to the binding site making it twist and escape the site more easily. Removing the benzene from thiazolium moiety seem to increase the binding constant if the double bond is kept. Dye **5**, however, requires much more space and has a weaker DNA binding, due to the missing double bond in the thiazolium moiety.

Two of the best dyes, **1** and **6** were selected for further studies with cellular RNA to prove that these monomethine cyanine dyes can be used to image both DNA and RNA.

Both dyes **1** and **6** do emit when bound to RNA. The intensity of dye **1** in complex with RNA is noticeably lower compared to its intensity when bound to DNA as shown in Fig. 5. Only very slight lowering of intensity can be observed for dye **6** when bound to DNA as compared to RNA. Emission maxima of dye **6** shifts from 492 nm to 496 nm in RNA solution. Interestingly, dye **6** shows a two-fold increase in intensity when

Table 2
Binding related data based on McGhee Von Hippel equation [20] (see Fig. S24 and Fig. S25. for related plots).

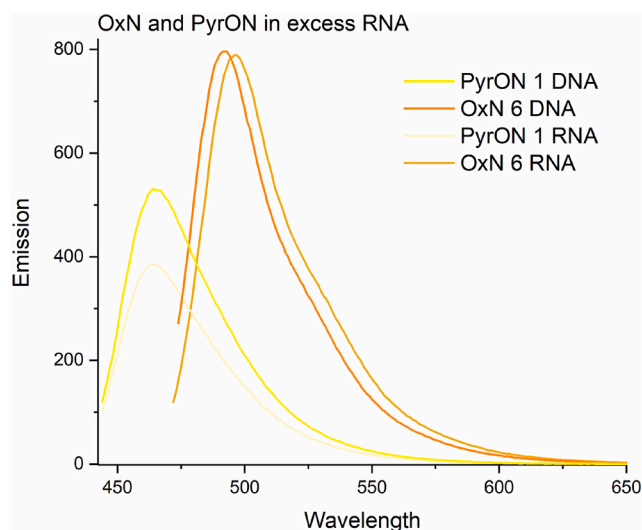| Dyes	Ka (x10^6 M^{-1})	Kd (nM)	n	ΔG^0 (kJ/mol)
PyrON **1**	1.2 ± 0.40	850	6.8 ± 0.30	−34.1
PyrN **2**	2.3 ± 0.20	441	4.2 ± 0.05	−35.7
QuinoN **3**	7.7 ± 0.20	129	1.9 ± 0.01	−38.8
QuinoS **4**	8.0 ± 0.90	124	1.7 ± 0.04	−38.9
QuinoN-2 **5**	2.2 ± 0.20	447	4.0 ± 0.20	−35.8
OxN **6**	8.5 ± 1.50	118	3.4 ± 0.40	−39.0
MeS **7**	4.6 ± 1.00	218	1.6 ± 0.04	−37.5
ThzN **8**	5.8 ± 0.40	171	2.1 ± 0.12	−38.1
ThzS **9**	2.3 ± 0.04	441	1.7 ± 1.00	−38.1

Fig. 5. Dyes **1** and **6** in excess cellular RNA in TE buffer solution. Dye concentrations were 0.3 μM for all four measurements. Dye **1** was excited at 436 nm and dye **6** at 464 nm.

bound to RNA compared to dye **1**, the only difference being the presence/absence of the benzene ring from the quinoline moiety. Both dyes **1** and **6** are suitable for both DNA and RNA detection.

3.3. Binding mode prediction and dynamics of DNA-dye complexes

In order to identify the specific DNA-dye interactions, molecular docking calculations were performed for dyes 2, 6, and 7. As observed in Fig. 6., all three dye molecules bind to AT-rich minor groove with calculated binding energies of -10.58 ± 0.04, -8.65 ± 0.57, and -8.88 ± 0.03 kcal/mol (average of ten lowest energy conformations; see Fig. S29) for dye 2, 6, and 7, respectively. The main contacts established between the dye molecules and nucleotides were lone pair–π, hydrogen bonds, and sulfur–π interactions (Fig. 6.). In all complexes, the heteroatom from the oxa/thia moiety is observed inside the minor groove; however, this atom contributes to the binding affinity only in dye 2. In contrast, in dyes 6 and 7, the interaction with the nucleotides is formed through the R3 ring, which also tends to be inside (Fig. 6).

As a further step, we investigated the dynamics of the (fully flexible) complexes in explicit solvent by mimicking the experimental conditions

to see if the DNA somehow induces a rigidity of dye molecules after complex formation. Molecular dynamics (MD) simulations showed the same binding site observed in docking calculations. The orientation of the dye molecules is parallel to the DNA strands throughout each MD simulation, and no intercalation between the base pairs is observed (see Supplementary Videos). Even though the dye molecules explore different regions of the DNA, they prefer to stay in the minor groove where the more significant interactions are stacking contacts (Fig. S30). The rigidity increases significantly (10–20 times) when dye molecules are bound to DNA compared to their free form, as shown in RMSD plots (Fig. 7). And more importantly, our results suggest that the movement restriction in the binding region as a result of this rigidity could be crucial for improving the brightness of the dyes. This is illustrated in Fig. 7, where the center of mass motion of the different dyes along the DNA shows a different binding site flexibility. Although dye 6 showed the lowest calculated binding affinity (from rigid docking), its behavior under more dynamic conditions shows that it is capable of forming the most stable complex with a low degree of fluctuation over the simulated period, which might explain the highest fluorescence observed experimentally.

Supplementary video related to this article can be found at https ://doi.org/10.1016/j.dyepig.2022.110844

4. Conclusions

Five new cyanine dyes (**1**–**5**) were synthesized and their photophysical properties were compared to previously published dyes (**6**–**9**) to gain a deeper understanding of which structural changes make these dyes better fluorescent probes for nucleic acids. Measured data clearly shows that a benzene ring at the thiazolium moiety plays a key role, and removing it lowers the brightness of the dyes drastically, making them too weak to be useable. This is not the case for removing a benzene ring from the quinoline moiety since it does not affect the brightness as strongly. As already discussed earlier [15] dyes with an oxazolium moiety or dimethylamine arm were brighter compared to dyes with thiazolium moiety or with methanethiol substituent. The molar absorption coefficients, which are used to determine how bright the dyes are, were the highest for each dye in ethanol suggesting that when dyes are fully solubilized their brightness is maximized. Hence enhancing water solubility could be one pathway to brighter dyes. Interestingly, the molecular docking calculations to identify the specific DNA-dye interactions showed that dye molecules **2**, **6** and **7** bind to the AT-rich minor groove and the main contacts established between the dye molecules and nucleotides were lone pair–π, hydrogen bonds, and sulfur–π
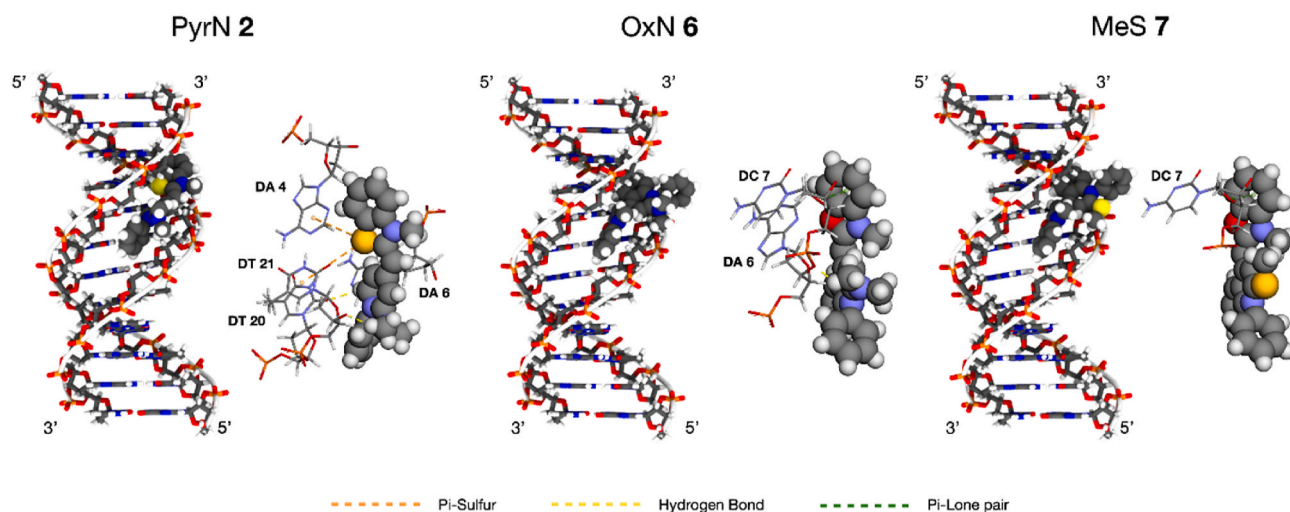

Fig. 6. Best docked conformations of PyrN **2**, OxN **6**, and MeS **7** dyes bound to B-DNA. For each complex, a full view of the binding site (left) and the main interactions established with nucleotides (right) are shown.
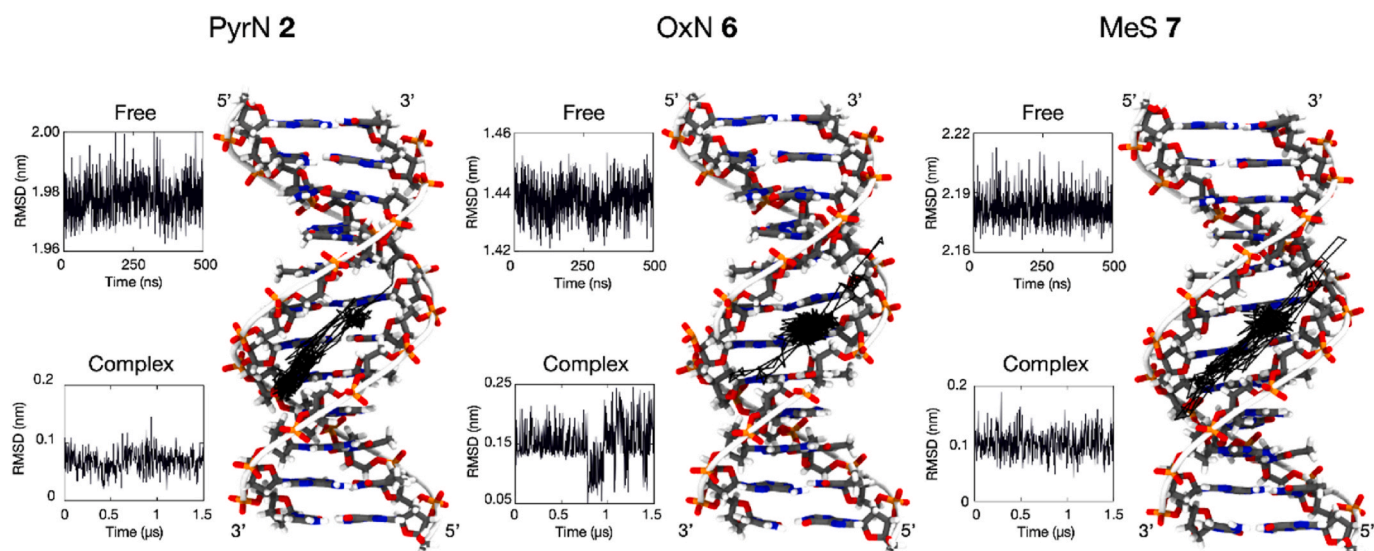
Fig. 7. Root mean square deviation (RMSD) of PyrN **2**, OxN **6**, and MeS **7** dyes in free form and in complex with B-DNA during simulated time. Black lines inside the B-DNA fragments represent the center of mass motion of the different dyes along the strands during the 1.5-µs MD simulation.

interactions. The structures **1**, **2**, **6**, **8** and **10** (due to a mixed composition, **10**, was not included in the photophysical studies) were determined by single crystal X-ray crystallography.

Our results give valuable information on how different structural modifications around the fixed fluorophore skeleton changes the nature and performance of these dyes. This information is crucial when new dyes are designed to obtain great brightness along with other desired traits such as better water solubility or even selectivity between DNA and RNA. The dyes discussed herein are currently being investigated with respect to their biological applications, including visualizing the virus uncoating in cells.

CRediT authorship contribution statement

Johanna M. Alaranta: Writing – original draft, Data curation, Formal analysis, Investigation. **Khai-Nghi Truong:** Data curation, Formal analysis, Investigation. **María Francisca Matus:** Writing – original draft, Data curation, Formal analysis, Investigation. **Sami A. Malola:** Writing – original draft, Data curation, Formal analysis, Investigation. **Kari T. Rissanen:** Writing – original draft, Data curation, Formal analysis, Investigation, Funding acquisition. **Sailee S. Shroff:** Data curation, Formal analysis, Writing, Investigation. **Varpu S. Marjomäki:** Data curation, Formal analysis, Writing, Investigation, Funding acquisition. **Hannu J. Häkkinen:** Writing – original draft, Investigation, Funding acquisition. **Tanja M. Lahtinen:** Writing – original draft, Data curation, Formal analysis, Investigation, Funding acquisition, Project administration.

Declaration of competing interest

The authors declare that they have no known competing financial interests or personal relationships that could have appeared to influence the work reported in this paper.

Data availability

No data was used for the research described in the article.

Appendix A. Supplementary data

Supplementary data to this article can be found online at https://doi. org/10.1016/j.dyepig.2022.110844.

References

[1] Shi H, Tan X, Wang P, Qin J. A novel near-infrared trifluoromethyl heptamethine cyanine dye with mitochondria-targeting for integration of collaborative treatment of photothermal and sonodynamic therapy. Mater Today Adv 2022;14:100251. https://doi.org/10.1016/j.mtadv.2022.100251.

[2] Wangngae S, Chansaenpak K, Weeranantanapan O, Piyanuch P, Sumphanapai T, Yamabhai M, et al. Effect of morpholine and charge distribution of cyanine dyes on cell internalization and cytotoxicity. Sci Rep 2022;12. https://doi.org/10.1038/s41598-022-07533-5.

[3] Li S, Wu Y, Liu S, Wu T, Liu G, Li T, et al. A multifunctional platinum(iv) and cyanine dye-based polyprodrug for trimodal imaging-guided chemo-phototherapy. J Mater Chem B 2022;10:1031–41. https://doi.org/10.1039/d1tb02682h.

[4] Ratto F, Magni G, Aluigi A, Giannelli M, Centi S, Matteini P, et al. Cyanine-doped nanofiber mats for laser tissue bonding. 2022. https://doi.org/10.3390/nano12091613.

[5] Liu L, Shi L, Liu J yong, wei Yang D, Fu Y, ying Ma X, et al. A cysteine and Hg2+ detection method based on transformation supramolecular assembly of cyanine dye by AGRO100. Spectrochim Acta Mol Biomol Spectrosc 2022;270:120779. https://doi.org/10.1016/j.saa.2021.120779.

[6] Heing-Becker I, Achazi K, Haag R, Licha K. Hydroquinone-functionalized cyanine dye as reduction-sensitive probe for imaging of biological reducing species. Dyes Pigments 2022;201:110198. https://doi.org/10.1016/j.dyepig.2022.110198.

[7] Aristova D, Kosach V, Chernii S, Slominsky Y, Balanda A, Filonenko V, et al. Monomethine cyanine probes for visualization of cellular RNA by fluorescence microscopy. Methods Appl Fluoresc 2021;9. https://doi.org/10.1088/2050-6120/AC10AD.

[8] Fei X, Gu Y. Progress in modifications and applications of fluorescent dye probe. Prog Nat Sci 2009;19:1–7. https://doi.org/10.1016/j.pnsc.2008.06.004.

[9] Shindy HA. Fundamentals in the chemistry of cyanine dyes: a review. Dyes Pigments 2017;145:505–13. https://doi.org/10.1016/j.dyepig.2017.06.029.

[10] Armitage BA. Cyanine dye–nucleic acid interactions. Top Heterocycl Chem 2008; 14:11–29. https://doi.org/10.1007/7081_2007_109.

[11] Kristinai L, Henary M. Cyanine dyes containing quinoline moieties: history, Synthesis, optical properties, and applications. Chem Eur J 2021;27:4230–48. https://doi.org/10.1002/chem.202003697.

[12] Mizuno Y, Watanabe K. Syntheses of cyanine dyes. Yakugaku Zasshi 1948;68: 250–2. https://doi.org/10.1248/yakushi1947.68.7-9_250.

[13] Dragan AI, Casas-Finet JR, Bishop ES, Strouse RJ, Schenerman MA, Geddes CD. Characterization of PicoGreen interaction with dsDNA and the origin of its fluorescence enhancement upon binding. Biophys J 2010;99:3010–9. https://doi.org/10.1016/J.BPJ.2010.09.012.

[14] Karlsson HJ, Eriksson M, Perzon E, Kerman AÊ, Westman G. Groove-binding unsymmetrical cyanine dyes for staining of DNA: syntheses and characterization of the DNA-binding. Nucleic Acids Res 2003;31:6227–34. https://doi.org/10.1093/nar/gkg821.

[15] Saarnio VK, Alaranta JM, Lahtinen TM. Systematic study of SYBR green chromophore reveals major improvement with one heteroatom difference. J Mater Chem B 2021;9:3484–8. https://doi.org/10.1039/d1tb00312g.

[16] Ying L. Nucleic acid detections and methods of their use. 2013. 2013/0137875.

[17] Saarnio VK, Salorinne K, Ruokolainen VP, Nilsson JR, Tero TR, Oikarinen S, et al. Development of functionalized SYBR green II related cyanine dyes for viral RNA detection. Dyes Pigments 2020;177:108282. https://doi.org/10.1016/j.dyepig.2020.108282.

[18] Karlsson HJ, Bergqvist MH, Lincoln P, Westman G. Syntheses and DNA-binding studies of a series of unsymmetrical cyanine dyes : structural influence on the degree of minor groove binding to natural DNA. Bioorg Med Chem 2004;12:2369–84. https://doi.org/10.1016/j.bmc.2004.02.006.

[19] IUPAC. Compendium of chemical terminology. In: The "Gold Book"). Compiled by A. D. McNaught and A. Wilkinson. second ed. Oxford: Blackwell Scientific Publications; 1997. Online version (2019-) created by S. J. Chalk., n.d.

[20] McGhee JD, von Hippel PH. Theoretical aspects of DNA-protein interactions: Co-operative and non-co-operative binding of large ligands to a one-dimensional homogeneous lattice. J Mol Biol 1974;86:469–89. https://doi.org/10.1016/0022-2836(74)90031-X.

[21] Brouwer AM. Standards for photoluminescence quantum yield measurements in solution (IUPAC technical report). Pure Appl Chem 2011;83:2213–28. https://doi.org/10.1351/PAC-REP-10-09-31.

[22] Benson RC, Kues HA. Absorption and fluorescence properties of cyanine dyes. J Chem Eng Data 1977;22:379–83. https://doi.org/10.1021/je60075a020.

[23] Zhang J, Moemeni M, Yang C, Liang F, Peng W-T, Levine BG, et al. General strategy for tuning the Stokes shifts of near infrared cyanine dyes. J Mater Chem C 2020;8:16769. https://doi.org/10.1039/d0tc03615c.

[24] Peng X, Song F, Lu E, Wang Y, Zhou W, Fan J, et al. Heptamethine cyanine dyes with a large Stokes shift and strong fluorescence: a paradigm for excited-state intramolecular charge transfer. J Am Chem Soc 2005;127:4170–1. https://doi.org/10.1021/JA043413Z.

[25] Dragan AI, Pavlovic R, McGivney JB, Casas-Finet JR, Bishop ES, Strouse RJ, et al. SYBR Green I: fluorescence properties and interaction with DNA. J Fluoresc 2012;22:1189–99. https://doi.org/10.1007/s10895-012-1059-8.

[26] Smith JG. Organic chemistry. fourth ed. New York: McGraw-Hill Education; 2014.

[27] Enkovaara J, Rostgaard C, Mortensen JJ, Chen J, Dułak M, Ferrighi L, et al. Electronic structure calculations with GPAW: a real-space implementation of the projector augmented-wave method. J Phys Condens Matter 2010;22:253202. https://doi.org/10.1088/0953-8984/22/25/253202.

[28] Perdew JP, Burke K, Ernzerhof M. Generalized gradient approximation made simple. Phys Rev Lett 1996;77:3865–8. https://doi.org/10.1103/PhysRevLett.77.3865.